Indian Journal of Chemistry
Vol. 64, January 2025, pp. 13-21
DOI: 10.56042/ijc.v64i1.13833

Energy-efficient synthesis of ZnO nanoparticles using white ash gourd fruit extract for their medicinal and environmental applications

Ravi Kant[a,b], Monika Chahar*[a], Anuj Mittal[b] & Seema[c]

[a] Department of Chemistry, Baba Mastnath University, Asthal Bohar, Rohtak 124 021, Haryana, India

[b] Department of Chemistry, M N S Government College, Bhiwani 127 021, Haryana, India

[c] Department of Chemistry, University of Rajasthan, Jaipur 302 004, Rajasthan, India

E-mail: chaharmonika507@gmail.com

Received 20 September 2024; accepted (revised) 27 December 2024

This work reports the green synthesis of ZnO nanoparticles (NPs) using white ash gourd fruit juice. The synthesized NPs have been characterized by various spectroscopic techniques like UV-Visible, FT-IR, Powder XRD and FE-SEM. These NPs display a prominent absorbance at 357 nm in UV-Visible spectra. X-ray diffraction studies confirm the formation of crystalline ZnO NPs with the wurtzite phase. The average particle size (D) of the synthesized ZnO NPs is found to be 40.48 nm. FE-SEM images reveal that synthesized ZnO NPs have nano-flaky structures. The prepared ZnO NPs have achieved 99% photodegradation efficiency against MB dye in 90 min of irradiation of UV light. These synthesized NPs have also been examined for three biological activities: Antimicrobial, antioxidant and anti-diabetic. Antimicrobial activity has been found to be good to moderate. The synthesized ZnO NPs show excellent anti-diabetic activity (α-amylase activity) compared to standard with IC_{50} value equal to 1.21 µg/mL. For α-glucosidase, green synthesized ZnO NPs (IC_{50} value 0.23 µg/mL) exhibit excellent inhibition activity compared to standard Acarbose (IC_{50} value 0.24 µg/mL). ZnO NPs show better antioxidant capability as well.

Keywords: Green synthesis, White ash gourd, Crystalline, Photocatalysis, Anti-diabetic, Antimicrobial

The invention and development of nanotechnology has revolutionized all walks of science, including biotech. Overtime, NPs have exhibited their influence and versatility in a wide range of sectors[1]. The scientific world is incredibly interested in them due to their astonishing applicability in numerous fields and businesses, including pharmacy, agro, and the food industry[2]. These days, extensive research has been going on regarding using metal oxide NPs (MONPs) for photodegradation processes and water purification[3–10]. These MONPs encompass CuO NPs, MgO NPs, ZnO NPs, TiO_2 NPs, Fe_2O_3 NPs, and Fe_3O_4 NPs[7,11,12]. More active sites and a large surface area on MONPs specifically facilitate rapid reaction times and improved product yields. Metal oxide NPs have been used to model relatively stable electrochemicals and biosensors with improved sensitivity and quicker responses[13–19].

ZnO NPs, compared to other MONPs, have drawn a great deal of focus owing to their unique physicochemical characteristics and biological uses, including wound care, antimicrobial, anti-diabetic, antioxidant, antifungal, and antiviral capabilities[20–24]. ZnO NPs' distinctive characteristics, such as size, shape, crystallinity, and chemical makeup, demonstrated significant promise for biomedical applications. One can modify the mechanical, chemical, optoelectrical, and medicinal properties of ZnO NPs by adjusting their nanoscale size[25]. More precise and regulated preparation techniques have been developed, allowing for the construction of the material into thin films or 3D solid bodies[25].

ZnO NPs that are biocompatible have now been manufactured *via* a greener approach, which qualifies them for biomedical uses. The greener approach offers a reliable and environmentally beneficial strategy which avoids the creation of undesirable or hazardous byproducts[26]. Plus, it reduces the dangerous chemicals needed in chemical synthesis, producing ecologically risk-free and biocompatible nanoparticles[2]. Ultimately, natural chemicals found in plant extracts serve as reducing and capping agents, crucial for stabilizing the green-synthesized ZnO NPs and minimising the need for costly and harmful reagents[27]. Green ZnO NP synthesis is gaining popularity due to its cost-effectiveness, inherent environmental friendliness, and

prospective uses in biomedicine, among other domains. These factors make it a desirable subject for further investigation. In keeping with this pattern, the current study sought to create ZnO NPs by using the fruit extract of the white ash gourd (*B. hispida*) in a phytofabrication process. White ash gourd (*Benincasa hispida* (Thunb.) Cogn. (synonym:*Benincasa cerifera* Savi) belongs to the Cucurbitaceae family that has a lot of promise for the production of functional food. This plant is a form of monoecious vine that produces big green fruits[28–30]. The primary chemical constituents of white ash gourd fruits are glycosides, volatile oils, saccharides, flavonoids, proteins, vitamins, carotenes, minerals, uronic acid, and ß-sitosterin. It has been reported that active constituents, such as terpenes, flavonoids, cardio glycosides, and sterols, have antioxidant effects[30–32]. In traditional medicines, it has been used to treat intestinal worms, fever, kidney disease, neurological disorders, and coughs. White ash gourd's primary bioactive ingredients have anticancer, anti-inflammatory, and cytotoxic effects[29,31,33]. We searched a lot of literature using keywords such as White ash gourd and *B. hispida* but did not find any research article that uses juice of white ash gourd. To the best of our knowledge, it is for the first time that white ash gourd fruit juice has been used to synthesize ZnO NPs. The fruit extract's phytochemicals, such as flavonoids, sterols, saccharides, *etc*., aided in the creation of ZnO NPs with improved properties and surface characteristics, which in turn assist in the application of these nanoparticles.

Materials and Methods

Zinc acetate dihydrate, sodium hydroxide, double distilled water and ethanol were purchased from Sigma Aldrich. Every chemical and reagent was of analytical grade and utilized as such (no other purification).

Preparation of White Ash gourd fruit extract

Washed and rinsed the white Ash gourd first using tap water and then with distilled water. Cut it, and the seeds were removed. It was further chopped into little pieces and then put inside a blender to be crushed. Took 100 g of this crushed Ash gourd in a conical flask (1 L) and added 400 mL of distilled water. After that, this flask was heated at 80 °C for 20 minutes in a water bath. Cooled the solution and filtered it with Whatman filter paper. Filtrate with a greenish tint was produced.

Green synthesis of ZnO NPs

5 g zinc acetate dihydrate and 40 mL extract of white ash gourd mixed in a beaker and stirred for 45 minutes at RT. Added 2N NaOH until its *p*H became 10-11. Continued stirring for 60 minutes at 80 °C. Then, white precipitates were obtained. Then, the precipitates were cooled down and filtered. Afterwards, rinse thrice with water that was double-distilled and twice with ethanol. The drying process of the precipitates was done in the oven by heating for 3-4 hours at 85°C. Consequently, a white-coloured powdered form was produced, which was utilized for additional testing and characterization [34].

Characterization

The synthesized NPs were characterized by UV–visible and FTIR spectroscopy, Powder XRD and FE-SEM. Using a PerkinElmer spectrophotometer (Lambda-750), UV–Vis absorption spectrum was recorded in the 200-800 nm range. The presence of different (functional) groups was certained by acquiring the spectrum using an FTIR spectrophotometer (PerkinElmer) within the range 4000–400 cm^{-1} using KBr pellets. The sample's XRD pattern was taken by a Panalytical X Pert Pro diffractometer. It was carried out between 10 to 80° with steps of 2°/min. An analysis of the sample's morphology was conducted by FESEM (Nova Nano 450-FEI).

Photocatalytic Study

To calculate the photodegradation efficiency of the sample, Methylene Blue (MB) dye decolorization under light irradiation was used. The initial concentration of MB dye solution taken for the said study was 5 ppm. Essentially, the adsorption-desorption equilibrium was established by dispersing the ZnO NPs (50 mg) in MB solution (150 mL) and stirring it for an hour in the dark. This mixture was put into a photocatalytic reactor (double-jacketed) that had a magnetic stirrer and a 250 W xenon lamp installed. The system was kept at the ambient temperature employing water circulation. 2 mL of the mixture was collected at various times and centrifuged for the purpose of separating the catalyst. The dye concentration was assessed by measuring the absorbance of the supernatant liquid using a UV–visible spectrophotometer.

The following formula was used to get the dye degradation rates:

Table 1 — Antimicrobial activity (inhibition zone in mm diameter) of synthesized ZnO nanomaterials

Compd name	Bacterial strain								Fungal strain			
	Gram +ve				Gram –ve							
	S. aureus				*E. coli*				*C. albicans*			
	20	40	60	80	20	40	60	80	20	40	60	80
	(µg/mL)				(µg/mL)				(µg/mL)			
ZnO NPs	6	9	11	13	N	7	10	12	N	8	12	13
Standard (40 µg/mL)												
Ciprofloxacin	30				32							
Ketoconazole									24			

$$\text{Degradation efficiency } = \frac{C_0 - C_x}{C_0} \times 100$$

where C_0 indicates the dye's initial absorbance and C_x indicates the dye's absorbance after a defined time.

Pseudo-first-order kinetics (Langmuir–Hinshelwood mechanism) is often followed in the photocatalytic degradation of organic dyes. The following pseudo-first-order equation was employed to study the kinetics of the degradation (photocatalytic) of MB dye:

$\ln (C_t/C_0) = -kt$,

Here, initial concentration and concentration at t time of light exposure are denoted by C_0 and C_t, respectively, and the rate constant is denoted by k (min^{-1}). Plotting $-\ln (C_t/C_0)$ against time (t) yielded a straight line whose slope indicated the rate constant of the photodegradation.

Biological activity

Antimicrobial activity

Using the Agar Well-Diffusion method, the antimicrobial potential of the prepared NPs was evaluated against *S.aureus*, *E. coli* (bacterial strains) and *C. albicans* (fungal strain). Mueller Hinton agar no. 2 (Hi-Media, India) and Sabouraud's dextrose agar (SDA) were used as the bacteriological and fungal medium, respectively. Dimethylsulphoxide (DMSO) was used to dilute the extract to a concentration of 10 mg/mL. The melted agar was then mixed in an aseptic manner with a standardized inoculum and transferred onto sterile Petri dishes to create a solid plate. The agar plates were made with wells, and a test substance was added to the well (6 mm) in quantities of 20, 40, 60, and 80 µL. The plates were kept at 98.6 ºF (37ºC) for the entire night. Zone sizes surrounding every single well were used to assess the extract's antimicrobial spectrum for each species of microbe. The agent's zone of inhibition was measured for its diameter and was compared against those of the commercial control antibiotics (ciprofloxacin and ketoconazole). Every step of the synthetic ZnO NPs antibacterial assay study was done in triplicate[35]. The outcomes of the related study are depicted in Table 1.

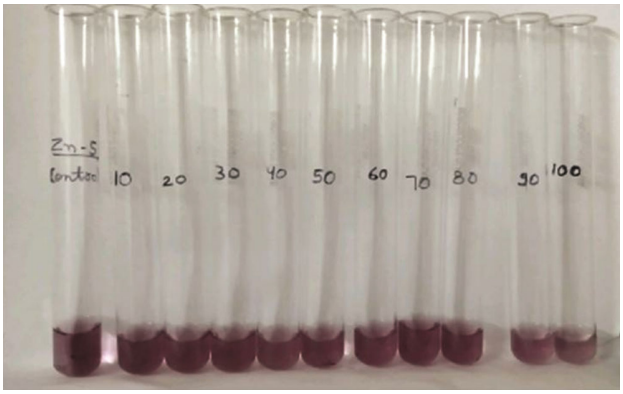

Fig. 1 — Different concentration solutions of compounds used for DPPH assay

Antioxidant activity

The green synthesized NPs were examined in reference to antioxidant potency through the DPPH assay, which is primarily used to investigate the nanomaterials' capacity to scavenge radicals[36].

DPPH method

The Prepared NPs' antioxidant capacity was examined by increasing their concentrations from 20 mg/mL to 100 mg/mL across the two samples. Samples were collected in Eppendorf and prepared in different concentrations ranging from 10 to 100 µl of sample and made up the volume to 1 mL with methanol (Fig. 1). Each sample was combined with 1 mL of DPPH in all series one by one, and vortex it. Following that, each sample was incubated at 37°C for 30 minutes. Methanol was used as a Blank. All samples' colour changes were tracked, and samples' absorbance was assessed using UV–visible spectra with a λ_{max} = 517 nm. For every sample, the data was

taken thrice. In the trial, standard ascorbic acid served as a reference for antioxidants. The ability of synthesized ZnO NPs to scavenge free radicals (%) was assessed as follows:

Blank – methanol and Control – methanol + DPPH (1:1)

$$\% \text{ DPPH scavenging activity } = \frac{A_C - A_S}{A_C} \times 100$$

Where A_C = absorbance of DPPH control and A_S = absorbance in the presence of test sample

Anti-diabetic activity

Synthesized ZnO NPs' anti-diabetic potential was evaluated using 500 µg/mL concentrations. Using Acarbose as the standard, the anti-diabetic potency was evaluated using an *in vitro* α-glucosidase and α-amylase enzyme inhibition assay[37].

α-Amylase Assay

The DNS technique was employed to measure the activity of α-amylase. 500 µg of green synthesized ZnO NPs sample, 500 µL of 0.02 M Na_3PO_4 buffer with 6 mM NaCl, and 0.04 units of the α amylase arrangement were mixed. The prepared NPs' mixture solutions were then brooded for 10 minutes at 98.6 °F (37°C). Next, 500 µL of 1% starch arrangement disintegrated in 0.02 M Na_3PO_4 support was comprised. 1.0 mL of 3,5-Dinitrosalicylic acid (DNS) reagent then ceased the response. The test tubes were placed in a bath of boiling water for 5 minutes and then allowed to cool down to an ambient temperature. After adding 10 mL of distilled water to dilute the reaction mix, the absorbance at 540 nm was reported.

α-Glucosidase Assay

For five minutes, the 500 µL nanoparticles' sample was incubated at 37°C with 0.2 M Tris buffer (*p*H 8.0) and 1 mL of the starch substrate solution (2% w/v maltose or sucrose). For initiating the reaction, 1 mL of α-glucosidase enzyme (1µg/mL) was mixed; the test tubes then underwent incubation for 40 min at 95 °F (35 °C). 2 cc of 6N HCl was then added to halt the reaction. Thereafter, the colour intensity was estimated by measuring the absorbance at 540 nm. The control samples were made in a similar manner but without the nanoparticles of green synthesized ZnO NPs. The percent inhibition and the IC_{50} value were calculated. For estimating the activity, % inhibition was calculated using the formula as earlier:

$$I = \frac{Abs\ control - Abs\ sample}{Abs\ control} \times 100$$

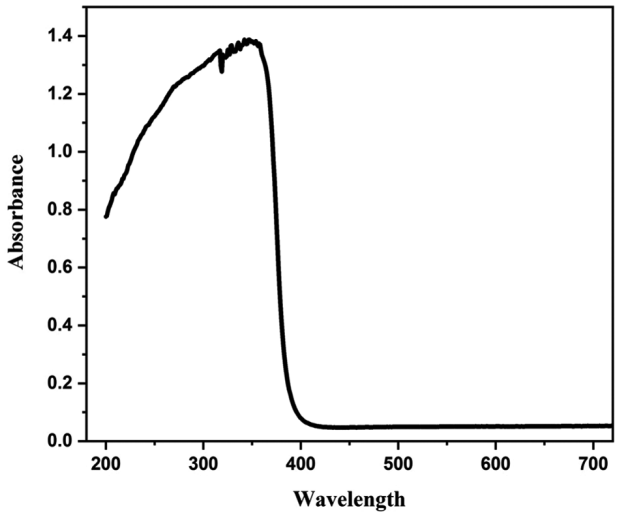

Fig. 2 — UV–visible spectra of synthesized ZnO NPs

Results and Discussion

UV–visible analysis

The UV-Vis spectrum of the synthesized NPs was taken in order to examine their absorbance and bandgap. It is shown in Fig. 2. The strong absorption peak at 357 nm confirms that ZnO nanoparticles were produced using a greener method[38]. Due to the shrinking of particles' size in the quantum confinement region, the absorption edge moved to a lower wavelength owing to larger band gap of particles[39]. Absorption spectra revealed the presence of an optical band gap of 3.47 eV, higher than bulk ZnO's 3.32 eV value. The following formula is used to determine the samples' band gap E_g[39].

$E_g = 1239.8/\lambda$

In our case,

$E_g = 1239.8 / 357$ nm = 3.47 eV

This value of band gap indicates the formation of smaller NPs[40].

Value of E_g is also estimated using Tauc Equation: $(\alpha h\nu)^{1/n} = K (E_p - E_g)$, where α denotes coefficient of absorption, v is the photon's frequency, h is Planck's constant, $E_p = h\nu$, E_g denotes band gap energy, K is constant and n being the power factor of transition mode, has the values ½ and 2 (allowed direct and indirect transitions), 3/2 and 3 (for forbidden direct and indirect transitions), respectively. The band gap (Eg) for ZnO is determined by plotting $(\alpha h\nu)^2$ *versus* hν and taking the extrapolated value for hν at α = 0. The value of E_g estimated for the synthesized ZnO is 3.26 eV (Fig. 3).

XRD investigation

XRD patterns of the synthesized NPs are depicted in Fig. 4. It clearly demonstrates XRD peaks, characteristics of ZnO nano-composite at 2θ = 31.98°, 34.65°, 36.48°, 47.76°, 56.85°, 63.03°, 66.18°, 68.04° and 69.12°. The planes (100), (002), (101), (102), (110), (103), (200), (112), and (201) are represented by these peaks. The above data confirmed the synthesized material to be ZnO, having a wurtzite phase. The peak pattern matched to the reported JCPDS card No. 36- 1451. Other than ZnO, no other notable peaks were seen[34]. The peaks obtained are strong and narrow, indicating good crystallinity[34]. The (100) plane associates with the perpendicularly aligned Zn-O bonds in the crystallite[41]. The well-defined peak pattern is a sign of good crystallinity of the synthesized sample[42]. The Debye-Scherrer's formula was used to find the crystallite size (*D*):

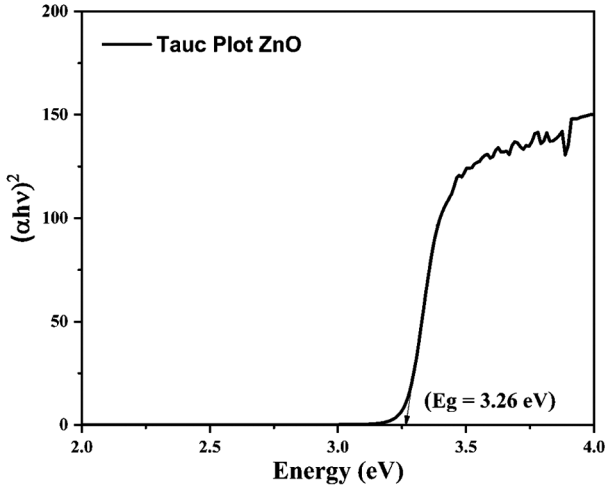

Fig. 3 — Tauc plot for synthesized ZnO NPs

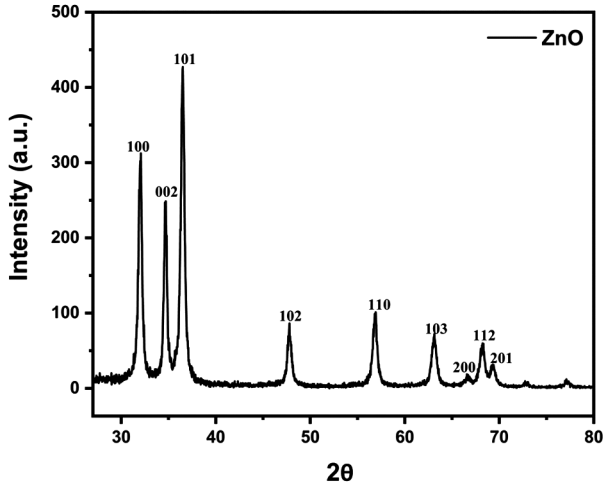

Fig. 4 — XRD plot of synthesized ZnO NPs

$$D = \frac{K\lambda}{\beta cos\theta}$$

where *D* denotes the size of crystallite (in nm), K (= 0.9) represents Scherrer constant, λ represents wavelength of the X-ray employed Cu Kα radiation (0.15046 nm), β denotes the FWHM for the most significant intense peak seen in the XRD pattern (at 2 θ = 36.48 for 101 plane) and θ denotes the Bragg's angle obtained from the 2θ value[43]. The average size (D) of prepared ZnO NPs is found to be in the range of 40.48 nm.

FTIR analysis

Fig. 5 presents the findings of the FTIR study and makes evident the presence of several functional groups. The peak at 3415-3400 cm^{-1} is indicative of O–H stretching[44]. It may also be attributed to the aromatic primary amine NH stretch.

The 2915 cm^{-1}peak denotes the C–H asymmetric stretch of the methylene group. The 1711 cm^{-1} peak confirms the C=O bond's presence, while the 1604-1594 cm^{-1} peak relates to the C=C stretch[45]. The peaks in the 400–650 cm^{-1} region indicate the metal-oxygen bonds (Zn-O bond)[46–48]. The phytochemicals contained in NPs may be responsible for the remaining peaks[28].

FESEM analysis

The surface morphology of synthesized NPs was mainly assessed by the FESEM analysis. It is indicated in Fig. 6 (a,b). The SEM investigation revealed that there was a significant level of dispersion in the nanoparticles. From the SEM images [Fig. 6(a,b)] of the synthesized samples, it can be seen that synthesized NPs have nano-flaky structures. Crucially, these structures are engineered

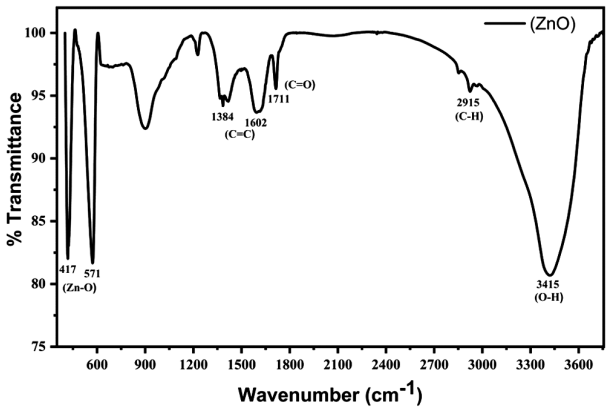

Fig. 5 — FTIR of synthesized ZnO

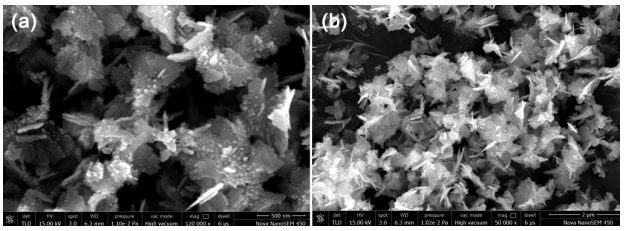

Fig. 6 — (a, b) SEM images of the ZnO NPs

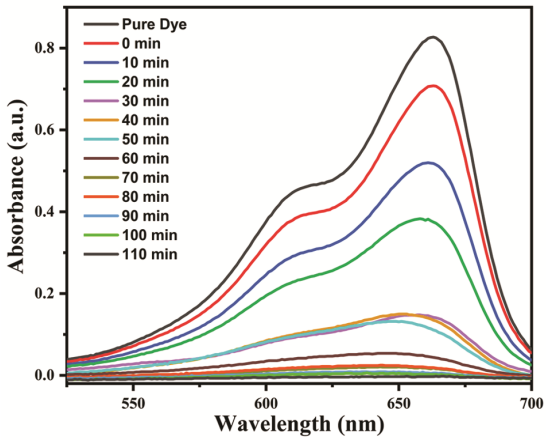

Fig. 7 — UV spectra of photodegradation of MB dye in the presence of ZnO NPs as photocatalyst

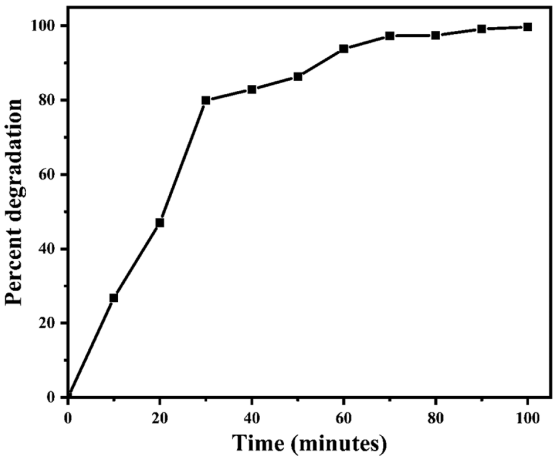

Fig. 8 — Percent degradation of MB dye with time using synthesized ZnO NPs

with a large number of pores of various sizes, which may act as transport channels for tiny molecules and enhance the material's chemical characteristics[49].

Photocatalytic analysis

Photodegradation of MB dye by ZnO NPs

Fig. 7 demonstrates the photocatalytic degradation of MB dye over green ZnO photocatalyst under UV light at RT for 110 min. The photodegradation is examined by noticing a substantial reduction of the

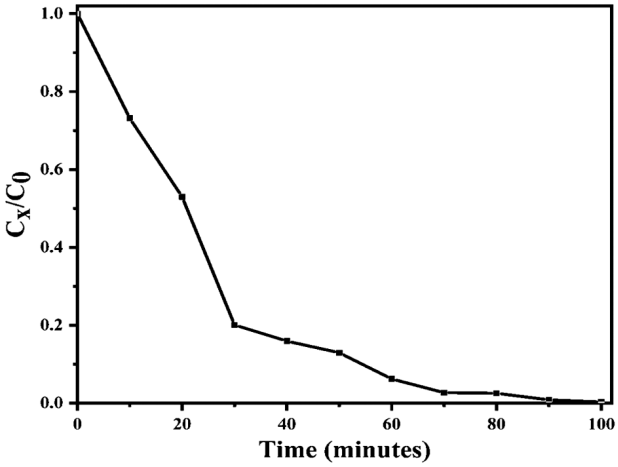

Fig. 9 — Variation of relative concentration of MB w.r.t. time using synthesized ZnO NPs

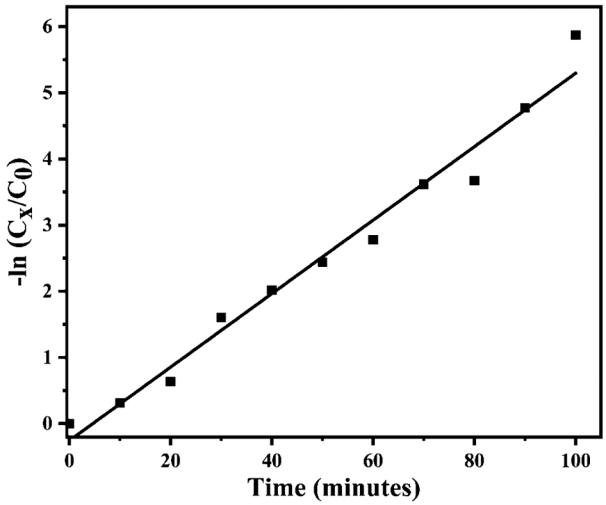

Fig. 10 — Degradation kinetic study of synthesized ZnO NPs

maximum absorption peak's (at 663 nm) intensity (over time) in UV spectra (Fig. 7). The prepared ZnO NPs exhibited 99% photodegradation efficiency in opposition to MB dye in 90 minutes of UV light irradiation (Fig. 8 and Fig. 9).

Kinetics of photo degradation

Kinetics of the degradation were studied by plotting a graph of -ln(*Cx*/*Co*) *vs*. time. Together with the rate constant, this graph (Fig. 10) also provides the regression coefficient's value, which is helpful in figuring out the kinetics and order of degradation. The graph is a straight line, with the regression constants' value above 0.95 and comparatively greater rate constant, as listed in Table 2.

As per Fig. 10, the photodegradation of MB dye over ZnO nano photocatalysts follows pseudo-first-order

Table 2 — Kinetics of the degradation MB dye over ZnO nano photocatalyst

Type of nanocatalyst	Rate constant (min^{-1})	Correlation coefficient (R^2)	Percent degradation in 90 min	Half-Life period
ZnO NPs	5.553×10^{-2}	0.97568	99	12.4977

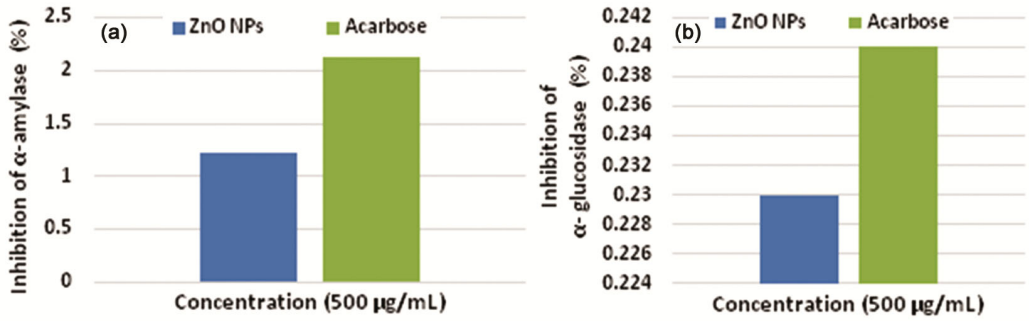

Fig. 11 — Anti-diabetic activity IC_{50} value of prepared ZnO *in vitro* (A) α-amylase (B) α-glucosidase

S. aureus *E. coli* *C. albicans*

Fig. 12 — Antimicrobial activity of green synthesized ZnO nanomaterials

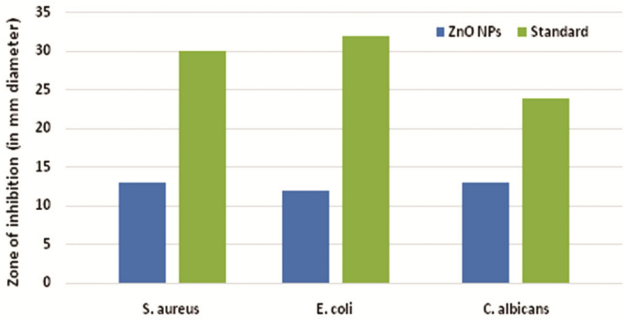

Fig. 13 — Bar diagram of antimicrobial activity showing maximum inhibition activity (in mm diameter)

kinetics, and the equation ln (C_t/C_0) = -kt (pseudo-first-order eqn.) matches the experimental findings quite well[21,41].

The value of rate constants (k) as calculated for the MB dye degradation employing ZnO NPs is 5.553×10^{-2}. This reflects that the synthesized ZnO NPs degraded MB dye more efficiently.

Biological activities

Antioxidant activity

The antioxidant potency of the ZnO NPs mediated by white ash gourd was studied by DPPH assays. In the DPPH assay, at 100 µg/mL, green-synthesized ZnO NPs exhibited antioxidant activity with 25.05%. Notably, the scavenging activity of synthesized NPs is dose-dependent, and its percentage increased with the increasing concentration. The lower IC_{50} (= 162.56 µg/mL) value indicated the superior antioxidant capacity of the white ash gourd ZnO NPs. The promising results of our inquiry provide a basis for further exploration into green produced ZnO NPs as a viable antioxidant option.

Anti-diabetic activity

The two digestive tract enzymes that catalyze the breakdown of starch and subsequent production of monosaccharides are α- glucosidase and α- amylase. Anti-diabetic assay of green synthesized NPs depicted in Fig. 11 exploring 15.23% (IC_{50} value 1.21 µg/mL) inhibition activity at 500 µg/mL concentration for α-amylase inhibition which has shown excellent efficiency compared to standard (IC_{50} value 2.11 µg/mL) whereas for α-glucosidase, green synthesized nano ZnO exhibited 44.1% (IC_{50} value 0.23µg/mL) inhibition action at 500 µg/mL concentration that explored good efficiency compared to standard Acarbose (IC_{50} value 0.24 µg/mL). Consequently, the exceptional ability of ZnO NPs to inhibit α-amylase and α-glucosidase, as demonstrated in the aforementioned outcomes, is indicative of their efficacy in the management of diabetes.

Antimicrobial activity

Making use of the standard Agar Well Diffusion method, prepared ZnO NPs were screened against bacterial strains(*S. aureus* and *E. coli*) and *C. albicans* (fungal strain). Ciprofloxacin and ketoconazole are used as standard antibiotics for antibacterial and antifungal activity, respectively. Fig. 12 and Fig. 13

show antimicrobial activity and maximum inhibition activity of greenly prepared ZnO NPs. Synthesized NPs exhibited good efficacy against *C. albicans* but were less effective against both bacterial strains.

Conclusion

This study represents the green synthesis of ZnO NPs using white ash gourd fruit extract. The UV-Vis spectrum of the synthesized nanostructures exhibited maximum absorption at 357 nm, and the band gap energy estimated using the Tauc plot was 3.26 eV. XRD validated the presence of crystalline nanoparticles of ZnO with hexagonal wurtzite formation and higher phase purity. The FESEM technique depicts nano-flaky structures with an average particle size of around 40 nm. The synthesized NPs exhibited 99% photodegradation efficiency of MB dye in 90 min of UV light irradiation in a neutral medium. The findings are consistent with the pseudo-first-order kinetic model. The developed NPs were also examined for antimicrobial, antioxidant, and anti-diabetic potential. These synthesized ZnO NPs (IC_{50} value 1.21 µg/mL) showed excellent anti-diabetic activity (α-amylase activity) as compared to standard (IC_{50} value 2.11 µg/mL). In relation to α-glucosidase, green synthesized ZnO NPs (IC_{50} value 0.23 µg/mL) exhibited excellent inhibition activity compared to standard Acarbose (IC_{50} value 0.24 µg/mL). Synthesized ZnO NPs (162.56 µg/mL) also showed better antioxidant capability. Antimicrobial activity was found to be good to moderate. The synthesized NPs exhibited good efficacy against fungal strain (*C. albicans*) but were less effective against both bacterial strains (*S. aureus* and *E. coli*). This investigation showed that the white ash gourd-mediated ZnO NPs can be used efficiently to break down the MB dye by photo degradation in contaminated water. The excellent potency of synthesized ZnO NPs against both α-amylase and α-glucosidase is a positive symbol of its effectiveness in diabetes treatment.

Acknowledgement

The authors are highly thankful to the Department of Chemistry, BMU Asthal Bohar, Rohtak, for providing the research facility.

Competing interests

None.

Funding

This research received no specific grant from public, commercial, or not-for-profit funding agencies.

References

1 Gadewar M, Prashanth G K, Babu M R, Dileep M S, Prashanth P A, Rao S, Mahadevaswamy M, Ghosh M K, Singh N, Mandotra S K, Chauhan A, Rustagi S, Yogi R, Chinnam S, Ali B, Ercisli S & Orhan E, *J Saudi Chem Soc*, 28 (2024) 101774.

2 Kumari S, Verma R, Chauhan A, Raja V, Kumari S & Kulshrestha S, *J Mat Today: Proc*, (2023) S2214785323021387. (https://doi.org/10.1016/j.matpr.2023.04.242)

3 Yadav S, Kumar N, Kumari V, Mittal A & Sharma S, *J Mat Today: Proc*, 19 (2019) 642.

4 Kumari V, Kumar N, Yadav S, Mittal A & Sharma S, *J Mat Today: Proc*, 19 (2019) 650.

5 Mittal A, Mari B, Sharma S, Kumari V, Maken S, Kumari K & Kumar N, *J Mater Sci: Mater Electron*, 30 (2019) 3186.

6 Mittal A, Sharma S, Kumari V, Yadav S, Chauhan N S & Kumar N, *J Mat Sci: Mat Elec*, 30 (2019) 17933.

7 Mittal A, Sharma S, Kumar T, Chauhan N S, Kumari K, Maken S & Kumar N, *J Mat Sci: Mat Elec*, 31 (2020) 2010.

8 Kumari V, Yadav S, Mittal A, Sharma S, Kumari K & Kumar N, *J Mat Sci: Mat Elec*, 31 (2020) 5227.

9 Karimi F, Rezaei-savadkouhi N, Uçar M, Aygun A, Tiri R N E, Meydan I, Aghapour E, Seckin H, Berikten D, Gur T & Sen F, *Food Chem Toxic*, 169 (2022) 113406.

10 Suresh D, Nethravathi P C, Udayabhanu, Rajanaika H, Nagabhushana H & Sharma S C, *Mat Sci Semicon Proc*, 31 (2015) 446.

11 Nikolova M P & Chavali M S, *Biomimetics*, 5 (2020) 27.

12 Fouda A, Eid A M, Abdel-Rahman M A, EL-Belely E F, Awad M A, Hassan S El-D, Al-Faifi Z E & Hamza M F, *Front Bioeng Biotech*, 10 (2022) 849921.

13 Petrucci R, Bortolami M, Di M P & Curulli A, *Nanomaterials*, 12 (2022) 959.

14 Liu G, Lu M, Huang X, Li T & Xu D, *Sensors*, 18 (2018) 4166.

15 Zahran M, Khalifa Z, Zahran MA-H & Azzem M A, *Mat Adv*, 2 (2021) 7350.

16 Bhalla N, Jolly P, Formisano N & Estrela P, *Essays Biochem*, 60 (2016) 1.

17 Ren X, Xu Z, Liu D, Li Y, Zhang Z & Tang Z, *Sensors Actuators B: Chem*, 357 (2022) 131384.

18 Li T, Yin W, Gao S, Sun Y, Xu P, Wu S, Kong H, Yang G & Wei G, *Nanomaterials*, 12 (2022) 982.

19 Singh H, Bamrah A, Bhardwaj S K, Deep A, Khatri M, Brown R J C, Bhardwaj N & Kim K-H, *Env Sci Nano*, 8 (2021) 863.

20 Jiang J, Pi J & Cai J, *Bioinorg Chem App*, 2018 (2018) 1.

21 Hatamie A, Khan A, Golabi M, Turner A P F, Beni V, Mak W C, Sadollahkhani A, Alnoor H, Zargar B, Bano S, Nur O & Willander M, *Langmuir*, 31 (2015) 10913.

22 Chandrasekaran S, Anusuya S & Anbazhagan V, *J Mol Struc,* 1263 (2022) 133139.

23 Asamoah R B, Yaya A, Mensah B, Nbalayim P, Apalangya V, Bensah Y D, Damoah L N W, Agyei-Tuffour B, Dodoo-Arhin D & Annan E, *Results Mat*, 7 (2020) 100099.

24 Pandey P, Packiyaraj M S, Nigam H, Agarwal G S, Singh B & Patra M K, *Beilstein J Nanotech*, 5 (2014) 789 .

25 Sirelkhatim A, Mahmud S, Seeni A, Kaus N H M, Ann L C, Bakhori S K M, Hasan H & Mohamad D, *Nano-Micro Lett*, 7 (2015) 219.

26 Rana A, Yadav K & Jagadevan S, *J Cleaner Prod*, 272 (2020) 122880.

27 Agarwal H, Venkat Kumar S & Rajeshkumar S, *Resource-Efficient Tech*, 3 (2017) 406.

28 Aromal S A & Philip D, *Physica E: Low-Dimel Sys Nano*, 44 (2012) 1329.

29 Soliman W E, Khan S, Rizvi S M D, Moin A, Elsewedy H S, Abulila A S & Shehata T M, *Nanomaterials*, 10 (2020) 1954.

30 Zaini NAM, Anwar F, Hamid AA & Saari N, *Food Res Int*, 44 (2011) 2368.

31 Islam M T, Quispe C, El-Kersh D M, Shill M C, Bhardwaj K, Bhardwaj P, Sharifi-Rad J, Martorell M, Hossain R, Al-Harrasi A, Al-Rawahi A, Butnariu M, Rotariu L S, Suleria H A R, Taheri Y, Docea A O, Calina D & Cho W C, *Oxi Med Cell Long*, 2021 (2021) 1.

32 Pahari N, Mahanti B, Banerjee M, Mandal K, Bhowmick B & Roy A, *Int J Health Sci*, 6 (2022) 844.

33 Baker A, Iram S, Syed A, Elgorban A M, Ahmad K, Khan S M & Kim J, *Int J Nanomed*, 16 (2021) 7711.

34 Meena P L, Poswal K & Surela A K, *Water Amp Env J*, 36 (2022) 513.

35 Dadi R, Azouani R, Traore M, Mielcarek C & Kanaev A, *Mat Sci Eng C*, 104 (2019) 109968.

36 Ahmed H E, Iqbal Y, Aziz M H, Atif M, Batool Z, Hanif A, Yaqub N, Farooq W A, Ahmad S, Fatehmulla A & Ahmad H, *Molecules*, 26 (2021) 4659.

37 Iqbal Y, Malik A R, Iqbal T, Aziz M H, Ahmed F, Abolaban F A, Ali S M & Ullah H, *Mat Letters*, 305 (2021) 130671.

38 Lal R, Gour T, Dave N, Singh N, Yadav J, Khan A, Jain A, Agarwal L K, Sharma Y K & Sharma K, *Front Chem*, 12 (2024) 1370667.

39 Rajkumari N P, Rouf A, Dutta P & Goswami P, *Mat Sci Eng B*, 287 (2023) 116094.

40 Alharthi F A, Alghamdi A A, Alothman A A, Almarhoon Z M, Alsulaiman M F & Al-Zaqri N, *Crystals*, 10 (2020) 441.

41 Kumari N, Sudharsan V, Kutty T M, Jayan N & Bhatlu M L D, *Mat Today: Proc*, (2023) S2214785323036829. (https://doi.org/10.1016/j.matpr.2023.06.287)

42 Li B & Wang Y, *Superlatt Microstruc*, 47 (2010) 615.

43 Saravanakkumar D, Sivaranjani S, Kaviyarasu K, Ayesshamariam A, Ravikumar B, Pandiarajan S, Veeralakshmi C, Jayachandran M & Maaza M, *J Semicond*, 39 (2018) 033001.

44 Babita D T & Ahmaruzzaman M, *Advances in Waste Management,* (Springer Singapore, Singapore), 2018, p 525.

45 Sharma S, Upadhyay A, Yadav P R, Galib R & Prajapati P K, *Indian J Ayurveda lntegr Med*, 3 (2022) 69.

46 Meena P, Surela A & Poswal K, *J Water Env Nanotech*, 6 (2021) 196.

47 Černík M & Thekkae P V V, *Int J Nanomed*, 8 (2013) 889.

48 Saravanan R, Karthikeyan S, Gupta V K, Sekaran G, Narayanan V & Stephen A, *Mat Sci Eng C*, 33 (2013) 91.

49 Li B & Wang Y, *Superlatt Microstruc*, 47 (2010) 615.